COVERSHEET

Intensifying salinity intrusion in the Barataria Basin, 2010 to 2026: a coastward gradient in the rate of change

Aaron Wang*

Independent researcher, Katy, Texas, USA

*Corresponding author: Aaron Wang
aaronwang730@gmail.com

ORCID: https://orcid.org/0009-0003-7494-5066

Intensifying salinity intrusion in the Barataria Basin, 2010 to 2026: a coastward gradient in the rate of change

Aaron Wang

Abstract

The Barataria Basin, a shallow microtidal estuary in coastal Louisiana, has lost a substantial part of its wetland area and is exposed to increasing salinity intrusion as the Mississippi River remains leveed and relative sea level rises. Salinity conditions in this basin have been described, but whether the rate at which salinity changes varies spatially across the basin has not yet been established. In this study, we analyzed continuous salinity records of 54 stations from the Coastwide Reference Monitoring System across the basin between 2010 and 2026. We then expressed each station relative to a coastal reference station to remove basin-wide variability, estimated a trend for each station, and related those trends to distance from the Gulf shoreline and to potential candidate environmental drivers. The salinity ratio to the coastal reference increases at 46 of 54 stations, with the rate of increase declining with distance from the basin shoreline. The gradient was present before the basin-wide increase of the early 2020s and was amplified by it. Of potential drivers examined, only storm surge and changes in tidal amplitude remain associated with the saltening rates after adjustment for distance and multiple testing. These findings show where basin salinity exposure is concentrated and provide an observational constraint for process-based models of tidal exchange. Because exposure varies systematically with position across the basin, monitoring and restoration efforts can be targeted, and the same approach applies to other tidally influenced deltaic basins.

Keywords: Coastal wetlands; Spatial gradient; Salinity Intrusion; Mann-Kendall; Coastwide Reference Monitoring System; Mississippi River Delta

1. Introduction

Coastal Louisiana’s wetlands provide ecological and economic benefits by buffering storm surge, supporting one of the most productive fisheries in the United States (Chesney et al., 2000), and improving water quality (Cheng et al., 2020). The plants a wetland can support depend on the salinity of its water; Louisiana’s marshes are classified as fresh, intermediate, brackish or saline on that basis, so a lasting change in salinity changes the marsh classification itself (Visser et al., 1998).

The Barataria Basin is one of the most rapidly degrading basins in the delta, accounting for about a quarter of all land loss across the Mississippi Delta Plain (Couvillion et al., 2017; Edmonds et al., 2023). Its wetlands have been affected by the loss of river sediment behind artificial levees and by a gradual rise in salinity as relative sea level rises, which has shifted the distribution of marsh types (Khalifa et al., 2024).

Salinity in the basin has been studied from several directions. The long-term statistical record of Louisiana’s estuaries was examined by Wiseman et al. (1990), the drivers of salinity variability in Barataria by Hu et al. (2023), and the basin’s salinity gradient and its response to river floods and diversions by Das et al. (2012). Tidal propagation into the basin has also been characterized, and recent work reports that tidal attenuation has decreased, so tides now reach further inland than they did before (Kang and Xie, 2024). Salinity under future restoration scenarios has been modeled, with relative sea-level rise projected to raise salinity through the basin over the coming decades (Khalifa et al., 2024).

Salinity intrusion is not confined to this basin. It is becoming more prevalent in deltas and estuaries worldwide (Lee et al., 2025); its causes are difficult to separate, as sea-level rise, subsidence, reduced river discharge and channel change can each independently contribute to intrusion (Rahman et al., 2019). Low-lying microtidal deltas are especially exposed due to tides being able to propagate a long distance inland across flat terrain (Kang and Xie, 2025).

Although salinity conditions and tidal propagation in this basin have each been characterized, whether the rate at which salinity is changing varies systematically across the basin has not been established. This study addresses that gap using continuous salinity records from 54 stations of the Coastwide Reference Monitoring System (Steyer et al., 2003) across the basin between 2010 and 2026. Each station is expressed relative to a coastal reference to remove basin-wide variability. Then, a trend is estimated for every station, and the trends are related to distance from the Gulf shoreline and to a set of potential environmental drivers. The result is an observational description of where in the basin salinity exposure is concentrated.

2. Environmental setting

2.1. Geography of the Barataria Basin

The Mississippi Delta Plain, a region in South Louisiana, has built lands over thousands of years through episodic river flooding, sediment deposition, and channel avulsions (Day et al., 1997). However, land growth reversed in the twentieth century. Levees along the Mississippi River, built to protect New Orleans and the communities along the river, cut off the sediment that had maintained the marshes (Blum and Roberts, 2009). Furthermore, canal construction has altered the basin’s internal hydrology between the distributaries (Day et al., 2000).

Spanning an area of roughly 7100 square kilometers, the Barataria Basin is an interdistributary basin west of the Mississippi River delta, bounded by the Mississippi River to the east and north, Bayou Lafourche to the west, and the Gulf of Mexico to the south (Kang and Xie, 2025; Fig. 1).

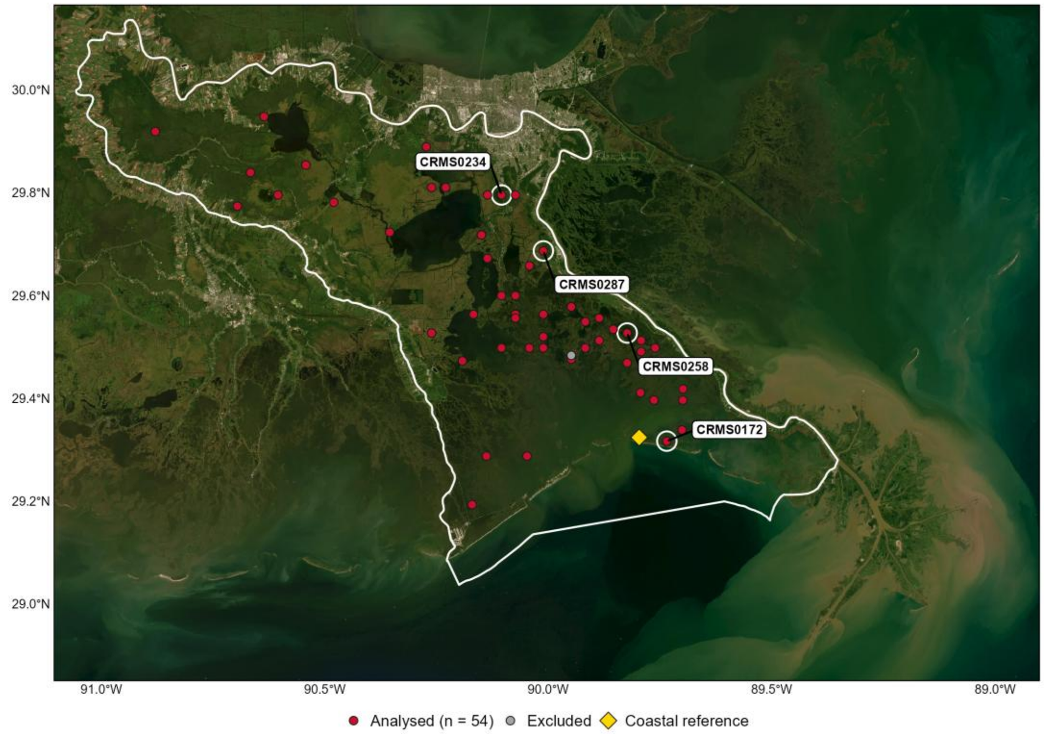

Fig. 1. Study area and monitoring network. The 54 Coastwide Reference Monitoring System stations analyzed (red circles), the coastal reference station (yellow diamond) and the one in-basin station excluded from analysis (grey) within the CPRA Barataria Basin boundary (white line). Ringed stations are those shown in Fig. 2. Imagery: Esri World Imagery.

Relief across the entire basin is about five meters, with natural levees along the river at four to five meters and marshes typically around sea level. The estuaries within the basin average about two meters deep (Inoue et al., 2008). The basin exchanges water with the Gulf of Mexico across its southern coastline through a small number of tidal passes and receives fresh water at its northern and inland areas. The basin is conventionally described in two areas: an upper region of fresh marshes and large lakes with minor tidal influence, and a lower region of brackish and saline marshes connected to the Gulf through tidal passes (Das et al., 2012).

2.2. Freshwater supply and tidal exchange

Salinity at any point within the basin is set by the balance between the fresh water arriving from the north and Gulf water entering through the tidal passes. Before artificial levees were constructed, natural levees of the Mississippi and Bayou Lafourche isolated the basin from the rest of the deltaic plain, with river water entering the basin only episodically. With the river now leveed along the eastern and northern boundary, fresh water arrives mainly through rainfall and runoff, with a controlled contribution from the Davis Pond Freshwater Diversion (Das et al., 2012). Freshwater supply is seasonal, with higher volumes occurring in the spring and lower volumes occurring in the summer; furthermore, during the summer, higher rates of evaporation also raise salinity (Wiseman et al., 1990). On the marine side, the coast is microtidal and diurnal (Kang and Xie, 2025). In a terrain of flat elevation, small tides propagate far inland. Relative sea level rises considerably faster here than the global rate because the land is also subsiding at an increasing rate (Byrnes et al., 2019). The result is an estuary in which mean salinity decreases from near-marine values at the coastline to fresh conditions in the upper basin over tens of kilometers (Fig. 2).

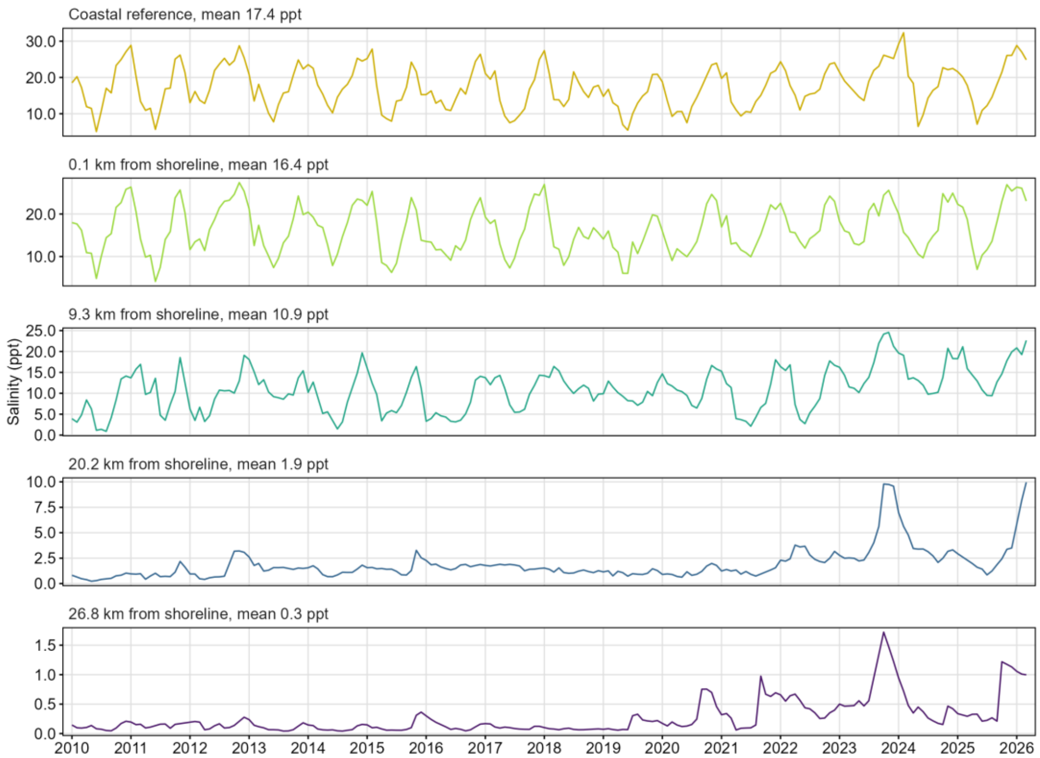

Fig. 2. Monthly mean salinity, 2010 to 2026, at the coastal reference station and at four analyzed stations from the shoreline inland, each panel on its own scale. Mean salinity falls by two orders of magnitude over about 27 km and month-to-month variability falls with it. The annual cycle dominates every record.

3. Data and methods

3.1. CRMS salinity data and station selection

To first analyze changes in local salinity levels, we used water data collected by the Coastwide Reference Monitoring System (CRMS), which collects hourly hydrographic data (Steyer et al., 2003). The variable analyzed was the CRMS Adjusted Salinity field, which is measured in parts per thousand (ppt); this is quality-controlled by the data provider CPRA (CPRA, 2022). We limited the data analysis period from January 2010 through March 2026 to ensure the most consistent operating times for the CRMS stations in the Barataria Basin. To specifically monitor salinity changes in the Barataria Basin, we limited the number of CRMS stations in our dataset from around 393 coastwide CRMS sites to an initial pool of 65 stations. We did this by clipping all 393 CRMS sites to the official CPRA hydrologic-basin boundary polygon for the Barataria Basin. The reference station, CRMS 0171, was chosen by screening the 21 stations nearest the Gulf on five criteria: a coefficient of variation in annual mean salinity below 15 percent, no significant trend over the study period ($p \geq 0.05$), no level shift larger than 10 percent, a mean salinity of at least 12 ppt, and at least 14 complete years of record. CRMS 0171 was the only station passing all five (mean 17.3 ppt, coefficient of variation 9.3 percent).

No values were interpolated or imputed. Furthermore, significant flagged spikes and flat runs were investigated against the provider documentation and were subsequently kept where physically consistent evidence was apparent.

Each CRMS Station data file consists of multiple sub-sensors, including the surface water, marsh, and well probes. To have the most consistent and significant salinity values, we decided to use only the stations with surface water probes (-H01), and we excluded marsh/well probes (-M01) since they do not record salinity, further reducing the number of CRMS stations from 65 to 57. Two additional stations were removed for having insufficient or incomplete data. Finally, we removed the reference station itself from the list of tested stations, as it is the ratio denominator, leaving a total of 54 stations for the subset. Afterwards, we ran a validity screening on the remaining CRMS stations' surface water probes, determining the percentage of hours that returned a valid salinity reading. We decided to fix the percentage that would constitute a valid salinity record at eighty percent or greater. All 54 stations passed the 80% validity threshold. For distance-gradient regression, two stations are excluded; they were relocated by the data provider in 2019 and their records after that point are published under the original identifiers. Using only the pre-relocation records truncates them relative to the rest of the roster, so only 52 stations are utilized for the gradient regression.

3.2. Salinity ratio

To calculate the salinity ratios, for each CRMS station in the subset, we aggregated hourly salinity into a monthly mean using all available hourly readings within each month. This was because hourly salinity carries tidal and weather fluctuations that are not part of a long-term trend. To quantify this, we computed the power spectral density of each station's hourly salinity record. Monthly aggregation also avoids timing lags in the salinity ratio: since the tide reaches the reference and inland stations at different times, hourly ratios would not be able to sufficiently detect salinity intrusion without timing noise from the tidal phase lag. Then, for each station i and month m, we computed the salinity ratio by dividing the station's monthly mean salinity by the reference station (CRMS 0171) in the same month. We used the equation,

$$S_i(m) = \frac{1}{n_i(m)} \sum_{k \in m} s_i(k) \tag{1}$$

$$r_i(m) = \frac{S_i(m)}{S_{\mathrm{ref}}(m)} \tag{2}$$

where $s_i(k)$ is the k-th valid hourly reading, $n_i(m)$ the number of valid readings in the month, $S_i(m)$ is the mean salinity of station i in month m, and S_ref(m) is the reference mean salinity in the same month. The ratio was defined for months in which both the station and the reference were able to return a valid monthly mean, with S_ref(m) being greater than zero. Since the reference station is most representative of the coastal salinity, ratios are generally near one for coastal stations and get progressively smaller inland in order to express each station's salinity relative to that at the coast. The purpose of analyzing salinity ratios was to remove basin-wide variability: if the entire basin were to increase or decrease proportionally in salinity in a given year, the ratio would be unchanged. However, an increase in a respective station's ratio shows that the station is increasing in salinity relative to the coast, which signifies salinity intrusion.

3.3. Trend estimation

Seasonal variations have a large effect on determining the trends of the salinity ratios, as such seasonal swings could mask the slow multi-year salinity intrusion. Because the seasonal cycle has a large effect relative to the trend, we used the Seasonal Mann-Kendall test, which compares each calendar month only with the same month in other years. Trends were computed in R (R Core Team, 2026) using the rkt package (Marchetto, 2024), which implements the Seasonal Kendall test. The method combines three components: the Mann-Kendall test for a monotonic trend (Mann, 1945), Sen's slope estimator for the magnitude (Sen, 1968), and the seasonal formulation that blocks by calendar month (Hirsch et al., 1982). Because it is rank-based and determines whether values tend to rise or fall between time points, it is insensitive to salinity spikes, data gaps, and the non-normal distributions common in salinity records. To have a consistent dataset, each station needed to have at least 10 monthly values spanning 2 different calendar months to be tested. Finally, we classified each station into three categories: saltening ($p < 0.05$ & slope > 0), freshening ($p < 0.05$ & slope < 0), or no significant trend ($p \geq 0.05$).

As a robustness check, we estimated each station's trend using a linear model with annual and semiannual harmonic terms. The long-term coefficient from each model provided a deseasonalized trend estimate, which was compared with the Seasonal Mann–Kendall result.

3.4. Distance to the shoreline and period comparison

Then, we wanted to find each CRMS station's distance from the shoreline in order to determine where the salinity intrusion actually lies within the basin. For this, we decided to use the true shortest distance to the shoreline (nearest point on the coastline) instead of a fixed transect line. Our coastline source was the Natural Earth medium-resolution (1:50m) shoreline (Massicotte and South, 2026), where we focused on the Louisiana coast bordering the Barataria Basin. All spatial processing was performed with the simple features (sf) package in R (Pebesma, 2018). The station coordinates and the Natural Earth coastline were reprojected from geographic coordinates to UTM Zone 15N (EPSG:26915), which is a projected coordinate system that reports distances in meters and minimizes distortion across the Barataria region. For each station, the shortest distance to the shoreline was computed as the minimum distance to the coastline geometry across all the segments. Next, we paired each station's distance with its trend rate to quantify the intrusion gradient. We were able to quantify it via linear regression of each station's Sen's slope against its distance to shore.

$$\hat{\beta}_i = \gamma_0 + \gamma_1 d_i + \varepsilon_i \quad (3)$$

where $\hat{\beta}_i$ is the Sen slope of station i, d_i is its shortest distance to the shoreline in kilometers, γ_1 is the gradient reported in Section 4.2, and ε_i is the residual.

To test whether drought could produce the gradient, each station's monthly ratio was first regressed on a calendar-month effect and the Palmer Drought Severity Index (Section 3.6), the seasonal Sen slope was taken from the residuals of that fit, and those drought-adjusted slopes were regressed on distance as in Eq. 3.

To describe how the salinity increase is distributed through the record, we computed the basin mean absolute salinity for each year on a fixed set of 50 stations reporting in every year from 2010 to 2025 with at least nine observed months in every year. This ensures that changes within the station set cannot produce an apparent shift in salinity level. On the same station set, each station's mean salinity over 2022-2025 was compared with its mean over 2010-2021. The boundary at the end of 2021 was taken from the annual series, in which every year from 2022 onward exceeds every earlier year.

3.5. Records before 2010

To determine whether the basin was saltening before 2010, we used two records that predate the continuous network. The first is a monthly transect of 48 stations from Grand Isle offshore to Bayou Chevreuil, sampled by hand from 1994 to 2016 (Turner, 2017), and the second is the Louisiana Department of Wildlife and Fisheries, which has recorded salinity at each trawl and seine sample since the 1960s (LDWF, 2019); we compared both records from 1994-2009. Both are grab samples, which are taken at the time of a site visit rather than continuously. We applied the same seasonal Mann-Kendall test, but with two different procedural changes. First, salinity ratio was not computed, as grab samples are not synchronous with any reference station. As a result, our pre-2010 trends are computed in absolute salinity and can contain potential basin-wide variability. Second, both historical records were screened for repeated readings and reporting-floor effects. No flagged observations met the criterion for exclusion, and each station month was represented by the median of its available visits.

3.6. Candidate drivers

To determine which environmental drivers are associated with the salinity trends, two comparisons were made. The first compares stations against one another and can detect only a cause that varies between stations; the second compares the basin against itself over time and can detect only a cause that varies through time. A driver may only be testable for one and not the other. For the spatial comparison, we report partial Pearson correlations after controlling for distance from the shoreline. Because the 17 driver constructs included 39 tested specifications, the Benjamini–Hochberg correction was applied across all 39 tests (Benjamini and Hochberg, 1995). Drought was represented by the Palmer Drought Severity Index for Louisiana climate division 5 from NOAA nClimDiv (Vose et al., 2014). Storm surge was measured from each station's hourly water level as the monthly maximum minus the monthly median, with storm months identified from the record and checked against the HURDAT2 best-track archive (Landsea and Franklin, 2013). River and diversion discharge were taken from U.S. Geological Survey gauges (National Water Information System).

Tidal amplitude at each station was measured from the station's own hourly water level as the interquartile range within each calendar month. We did this for stations with months that had at least 200 hourly readings. We chose the interquartile range because it describes the ordinary spread of water level and is insensitive to isolated extremes, so it responds to the tide and to sustained setup rather than to individual environmental events. A trend in monthly amplitude was estimated at each station with the same seasonal Mann-Kendall test utilized for salinity. Since the water-level record is shorter than the 18.6-year lunar nodal cycle, no basin-wide trend in amplitude is claimed. Therefore, the quantity used is the between-station contrast in amplitude trend.

To determine whether distance from the shoreline acts through tidal amplitude, a mediation model (Baron and Kenny, 1986) was used to estimate the share of the distance effect that passes through the amplitude trend.

4. Results

4.1. Basin-wide salinity trends

We analyzed the magnitude of salinity intrusion across 54 CRMS stations in the Barataria Basin from 2010 to 2026. After conducting Seasonal Mann-Kendall tests on the monthly salinity ratios for each station, we found that 46 stations had increased salinity ratios, 1 station had decreased salinity ratios, and 7 stations had no significant trend at $p < 0.05$ (Fig. 4). The monthly series are shown in Fig. 5. The same test on absolute salinity gives 44 rising, 3 falling and 7 no trend. The harmonic deseasonalization check produced the same trend directions; no station's trend was reversed. To confirm that the monthly aggregation is a necessary approach, we computed the power spectral density (PSD) of each station's hourly salinity. The tidal band holds a median 0.56 percent of each station's salinity variance, and periods of four months and longer hold 57.4 percent (Fig. 3).

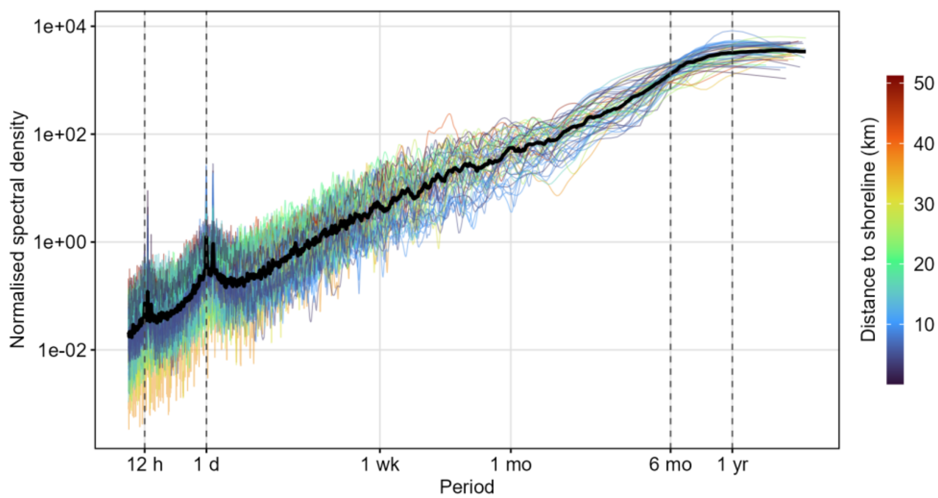

Fig. 3. Power spectral density of hourly salinity, one curve per station scaled to unit area, colored by distance to the shoreline, with the median across stations (black) and reference periods of one year, six months, one day and twelve hours (dashed). The tidal band (11.5 to 26 h) holds a median 0.56 percent of each station's variance; periods of four months and longer hold 57.4 percent.

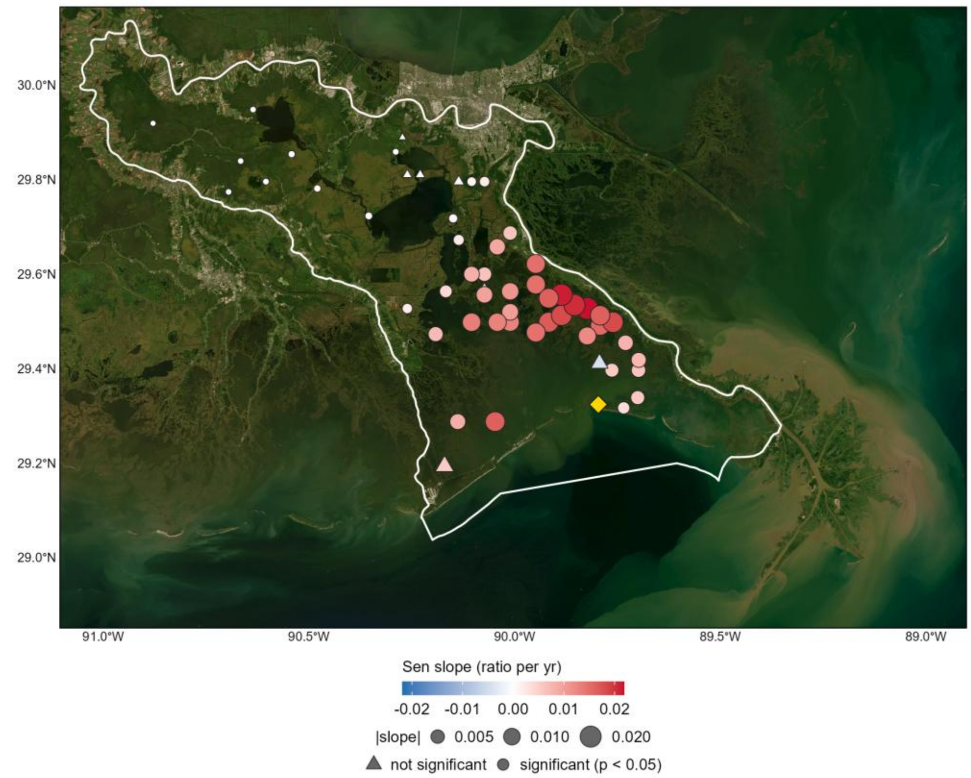

Fig. 4. Seasonal Mann-Kendall trend in the salinity ratio, 2010 to 2026, at each of 54 stations, color and size by Sen slope; circles are significant at $p < 0.05$ and triangles are not. The diamond marks the coastal reference. The ratio increases at 46 stations, decreases at 1, and shows no significant trend at 7.

Fig. 5. Monthly salinity ratio at the same 54 stations, offset vertically by distance from the shoreline, coastal at the bottom. The vertical scale is the offset order, not a ratio value.

4.2. Dependence of the trend on distance to the shoreline

To quantify how the saltening trends vary with position in the basin, each station's Sen slope was regressed against the shortest distance to the coastline. The regression gives a slope of −0.000338 ratio/year per km ($p = 2.4 \times 10^{-7}$, $R^2 = 0.42$, $n = 52$; Fig. 6a). Of the 52 stations, 47 have significant trends; the five that do not lie a mean 20.2 km inland against 14.0 km for the rest. The same regression on absolute-salinity slope gives -0.0062 ppt/year per km ($p = 7.5 \times 10^{-8}$, $R^2 = 0.44$, n = 52; Fig. 6b). To determine whether drought had a potential impact on the distance gradient, we regressed out the Palmer drought index, which increased the distance gradient to −0.000363 ratio/year per km ($p = 1.1 \times 10^{-7}$). On the record before the level shift, January 2010 to October 2021, the ratio gradient is −0.000190 ratio/year per km ($p = 0.0022$, $R^2 = 0.17$, n = 52; Fig. 7b), about half the full-record slope. Over that record 10 stations had a significant rising ratio, 3 falling and 41 no trend after Benjamini-Hochberg correction (Fig. 7).

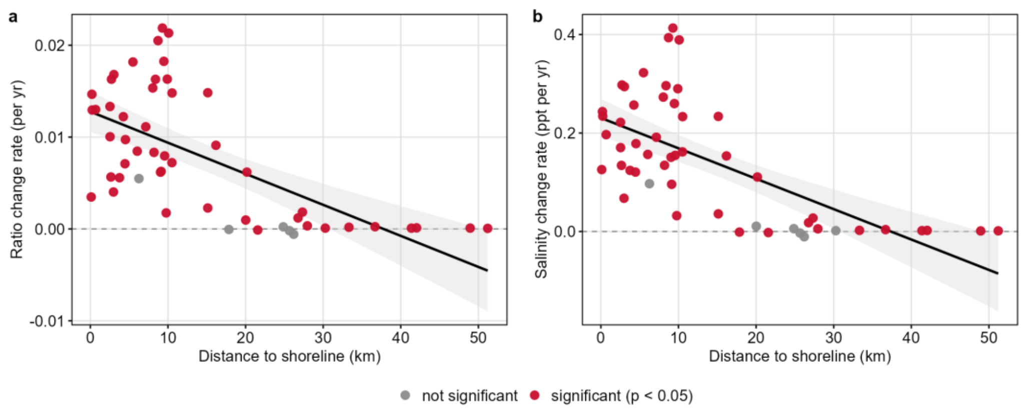

Fig. 6. Rate of change against shortest distance to the Gulf shoreline for the 52 stations of the gradient roster. (a) Sen slope of the salinity ratio; (b) Sen slope of absolute salinity. Red points are significant at $p < 0.05$, grey are not. Lines are ordinary least-squares fits with 95 percent bands. The ratio rate falls by 0.000338 per year for each kilometer inland ($p = 2.4 \times 10^{-7}$, $R^2 = 0.42$); the absolute rate by 0.0062 ppt per year per kilometer ($p = 7.5 \times 10^{-8}$, $R^2 = 0.44$). The gradient does not depend on the reference station.

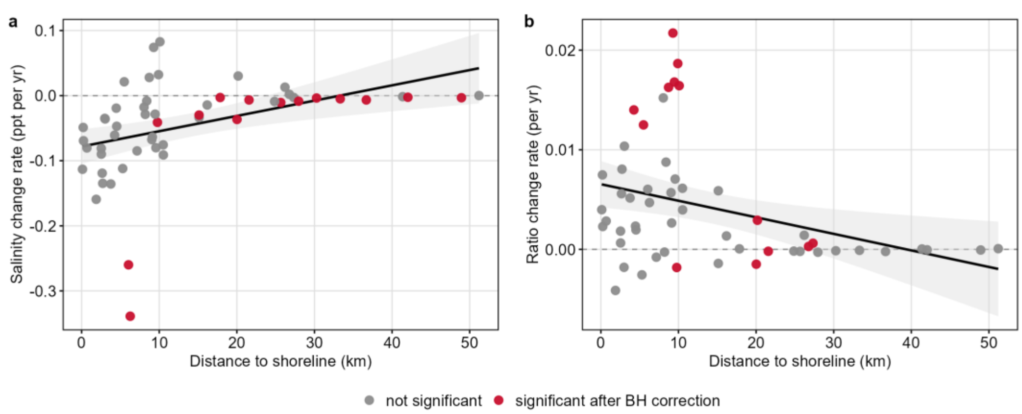

Fig. 7. Trends over the early record, January 2010 to October 2021, at all 54 stations. (a) Sen slope of absolute salinity against distance to the shoreline; (b) the same for the ratio to the coastal reference. Red points are significant after Benjamini-Hochberg correction. Absolute salinity: 0 saltening, 14 freshening, 40 no trend; ratio: 10 saltening, 3 freshening, 41 no trend. The contrast holds for any end month between June 2020 and June 2022. On the 52-station gradient roster the ratio gradient over this record alone is -0.000190 per year per km ($p = 0.002$, $R^2 = 0.17$).

4.3. Timing of the salinity increase

On the fixed set of 50 stations with at least nine observed months in every year, annual basin mean salinity in each year from 2022 to 2025 exceeded that in every year from 2010 to 2021 (Fig. 8a; Table 1). Each station's mean salinity was higher in the 2022-2025 block than in the 2010-2021 block, with a median difference of approximately 2.8 ppt. The increase falls with distance from the shoreline (Kendall's $\tau = -0.45$, $n = 50$; Fig. 8). These comparisons describe the observed record without estimating an onset date or attributing the increase to a particular driver.

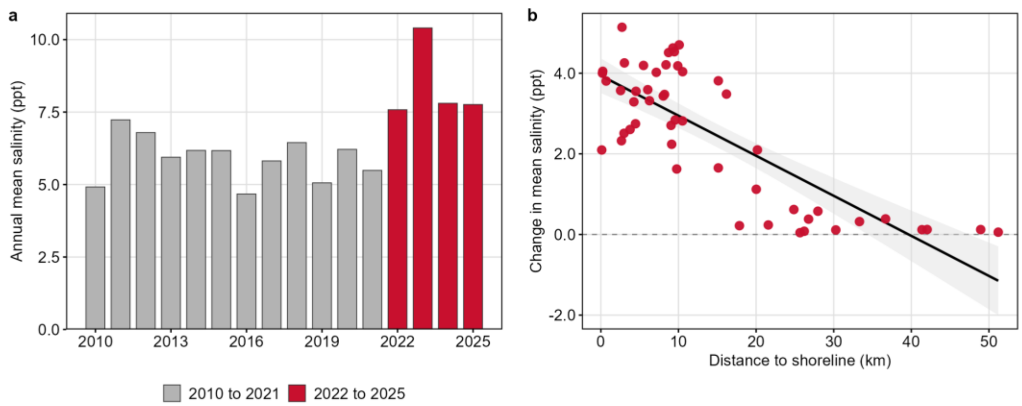

Fig. 8. The late increase in absolute salinity, on the 50 stations with at least nine months of data in every year 2010 to 2025. (a) Annual mean salinity across those stations; every year from 2022 exceeds every year before it (4.67 to 7.23 ppt over 2010 to 2021 against 7.58 to 10.40 ppt over 2022 to 2025). (b) Each station's mean over 2022 to 2025 minus its mean over 2010 to 2021, against distance to the shoreline: 50 of 50 positive, median +2.78 ppt, about 3.6 ppt within 15 km and 0.1 ppt beyond 25 km (Kendall's tau = -0.451, $p = 3.9 \times 10^{-6}$). The line is the least-squares fit. The later block includes the 2022 to 2023 drought.

Table 1. Basin salinity year by year, 2010 to 2025, all 54 stations; 2026 is excluded (three months). Median ratio and median salinity are medians across stations of each station's annual mean. The level gradient is the least-squares slope of annual-mean ratio on distance to the shoreline within that year, a gradient of level rather than of rate. No onset year is inferred from this table; the paper's trend evidence is the per-station test, not the annual series.

Year	Stations	Median ratio	Median salinity (ppt)	Level gradient (ratio per km)	p	R2
2010	52	0.226	3.43	-0.0146	3.4e-06	0.35
2011	52	0.503	7.13	-0.0219	4.2e-09	0.50
2012	54	0.267	5.73	-0.0156	7.8e-08	0.43
2013	54	0.226	3.83	-0.0169	5.0e-07	0.39
2014	54	0.276	5.14	-0.0158	1.2e-07	0.42
2015	54	0.291	4.98	-0.0170	1.1e-07	0.42
2016	54	0.192	3.22	-0.0133	8.8e-07	0.37
2017	54	0.293	3.99	-0.0185	3.1e-07	0.40
2018	54	0.284	4.89	-0.0175	4.8e-08	0.44
2019	54	0.232	3.17	-0.0176	5.1e-07	0.39
2020	52	0.299	4.66	-0.0191	1.1e-07	0.43
2021	52	0.216	3.75	-0.0163	1.4e-06	0.38
2022	52	0.422	7.53	-0.0193	9.6e-09	0.49
2023	52	0.587	12.75	-0.0224	5.1e-12	0.62
2024	52	0.409	6.71	-0.0201	1.2e-09	0.53
2025	52	0.417	6.98	-0.0212	3.3e-09	0.51

4.4. Salinity before 2010

Annual salinity was elevated from 1999 to 2007, peaking in both 2000 and 2006. Despite covering different areas of the basin and differing in mean salinity, the Turner and LDWF records agree closely on this pattern (r = +0.966, n = 16 years). Over 1994–2009, no station in either record had a significant trend after Benjamini-Hochberg adjustment. The earliest data from the CRMS continuous network also reproduces the same result: between May 2007 and December 2009, none of 40 stations were saltening.

4.5. Tidal amplitude and other drivers

The change in tidal amplitude predicted the saltening rate approximately as well as distance (R^2 = 0.413 versus 0.417; Fig. 9). Both links of the mediation model were significant: distance was associated with amplitude, and amplitude was associated with the saltening rate after controlling for distance. Adding amplitude to the distance model reduced the distance coefficient by approximately two fifths, consistent with amplitude accounting for part of the spatial association.

Across all 39 specifications, BH correction retained storm surge (partial r = +0.527, p = 0.0010) and the tidal amplitude trend (+0.489, p = 0.0026; Fig. 10; Table 2) among the interpretable drivers. In an exploratory model including shoreline distance, storm surge, and the trend in tidal amplitude (n = 54), the distance coefficient was not statistically significant (p = 0.331).

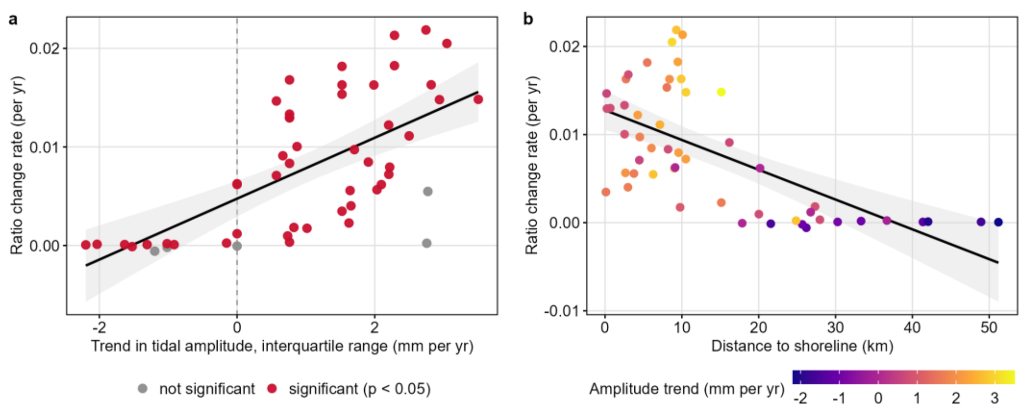

Fig. 9. What distance stands for, on the 52-station gradient roster. (a) Rate of change of the salinity ratio against the trend in tidal amplitude at the same station, measured as the interquartile range of hourly water level; red points are stations with a significant ratio trend. (b) The same rate against distance to the shoreline, colored by the amplitude trend. Amplitude predicts the rate about as well as distance does (R^2 = 0.413 against 0.417). In a mediation model both paths hold (distance to amplitude $p = 1.4 \times 10^{-8}$; amplitude to rate with distance held fixed p = 0.010), and roughly two fifths of the distance effect runs through amplitude, with a bootstrap interval of 9 to 81 percent.

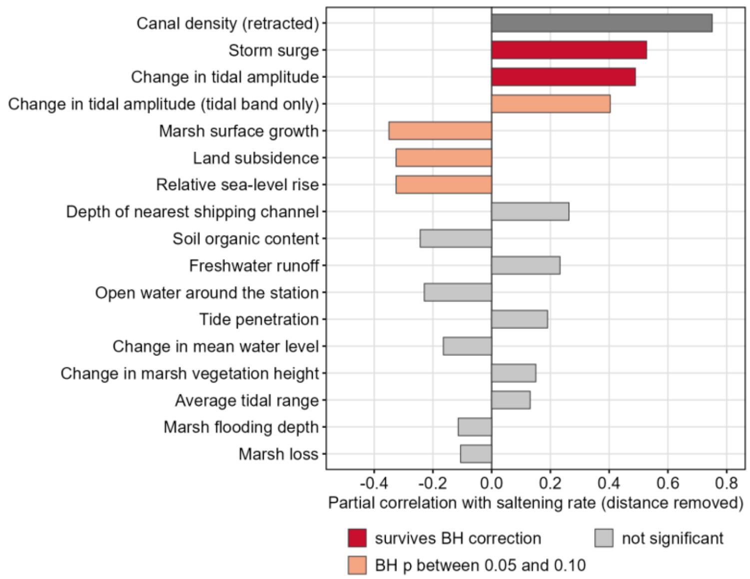

Fig. 10. Partial correlation of each of 17 candidate drivers with the station saltening rate after distance to the shoreline is removed from both, ranked by magnitude. Filled bars survive Benjamini-Hochberg correction at 0.05: storm surge (r = +0.53) and change in tidal amplitude (r = +0.49). The open bar is a canal-density result retracted as a mapping artifact and is shown so that all constructs tested appear (Table 2).

Table 2. Candidate drivers of the saltening rate, ranked by Benjamini-Hochberg corrected p. Partial r is the Pearson correlation between each driver and the station saltening rate after distance to the Gulf shoreline is removed from both; n is the number of stations with the driver available.

Driver	Measure	n	Partial r	p	BH p
Canal density a	Fraction of station area occupied by canals (National Hydrography Dataset)	35	+0.751	3.2e-07	5.4e-06
Storm surge	Water-level rise above the monthly median during storm months	54	+0.527	5.0e-05	4.2e-04
Change in tidal amplitude	Trend in the monthly interquartile range of hourly water level	54	+0.489	2.0e-04	0.001
Change in tidal amplitude (tidal band only)	Trend in amplitude of the 10 to 30 h water-level band	38	+0.404	0.013	0.053
Land subsidence b, c	Subsidence rate (Nienhuis et al., 2017)	53	-0.325	0.019	0.053
Relative sea-level rise b	Subsidence plus sea-level rise	53	-0.325	0.019	0.053
Marsh surface growth	Vertical accretion rate from marker horizons	43	-0.350	0.023	0.056
Depth of nearest shipping channel	Navigation channel depth	54	+0.263	0.057	0.121

Soil organic content	Organic matter fraction of marsh soil	54	-0.243	0.079	0.150
Freshwater runoff	Modeled surface runoff (TerraClimate)	54	+0.233	0.094	0.152
Open water around the station	Fraction of surrounding area that is permanent open water (JRC Global Surface Water)	54	-0.229	0.099	0.152
Tide penetration	Station tidal range divided by coastal tidal range	53	+0.190	0.177	0.250
Change in mean water level	Trend in monthly mean water level	51	-0.164	0.254	0.332
Change in marsh vegetation height	Trend in vegetation height	54	+0.150	0.283	0.343
Average tidal range	Mean monthly standard deviation of hourly water level	54	+0.131	0.349	0.396
Marsh flooding depth	Mean water level relative to the marsh surface	52	-0.114	0.427	0.451
Marsh loss	Change in surface-water occurrence within 5 km, 1984 to 1999 versus 2000 to 2021 (JRC)	54	-0.106	0.451	0.451

a Retracted: the association was traced to a mapping artifact in how canal length was attributed to stations. Retained so that all seventeen drivers tested are shown.
b Subsidence and relative sea-level rise are one underlying series counted twice.
c Estimator-dependent: the Kendall partial is +0.059 and the sign reverses. Storm surge and change in tidal amplitude are significant under both estimators.

5. Discussion

5.1. Intrusion from the shoreline

The rate at which salinity is increasing in the Barataria Basin declines with distance from the Gulf shoreline. This coastward concentration is consistent with stronger coastal influence. The gradient remained statistically significant and became steeper after adjustment for the Palmer drought index, indicating that the spatial association was not explained by the fitted Palmer drought index term alone.

The late rise shows the same pattern; it is the largest near the shoreline, about 3.6 ppt within 15 km of the shoreline and near zero beyond 25 km. The trend and the rise measure different areas, as one is a rate over sixteen years with ratio units, while the other is the size of a single increase in ppt. Both decrease with distance in the same method, and the agreement between them is what makes the spatial claim difficult to attribute to the choice of metric or window.

5.2. Absolute salinity and the ratio

The spatial structure is older than the recent increase in salinity; fitted to the record before the increase alone, we found that the rate of change in the ratio still declines with distance from the shoreline, so the pattern was present before the basin-wide salinity increase and was consequently amplified by it.

The increase is not evenly distributed through the study period. In absolute salinity, the basin freshened slightly through much of the 2010s before rising sharply in the final years. Meanwhile, measured as a ratio to the coastal reference, the same period shows no such decline. The ratio was generally flat to increasing over 2010–2021 and increased over the full record. The late-period block comparison separately shows higher absolute salinity during 2022–2025 than during 2010–2021. The difference arises because absolute salinity is controlled by how much fresh water the basin receives, which was comparatively high from 2017 to 2021. The ratio removes such basin-wide effects and focuses on the relationship between inland stations relative to the coast. The two separate metrics together indicate that inland stations are slowly becoming more coast-like over the study period. In the ratio, this appears as a modest increase in the 2010s, followed by a larger increase in the later record; on the earlier record alone, only 10 of the 52 stations had a significant rising ratio, against 46 stations over the full record.

The records before 2010 indicate that the study period does not begin partway through a longer increase. The two independent salinity networks both demonstrate that salinity was elevated from approximately 1999 to 2007 and subsequently returned to earlier levels. This indicates that the increase reported is specific to the study period rather than a continuation of salinity intrusion already in process.

5.3. Tidal amplitude as a candidate mechanism

Distance is a coordinate and cannot physically act as a driver, so it must represent a physical driver that varies with it. Tidal amplitude showed the strongest association with the spatial salinity change pattern. The interquartile measure describes the ordinary spread of water level and, unlike the full range, is relatively insensitive to isolated extreme events. However, it includes tidal and non-tidal variability and therefore should not be interpreted as a direct measurement of tidal forcing alone.

These results can be reconciled with earlier work in the same basin. Kang and Xie (2024) reported reduced tidal attenuation, consistent with farther inland propagation of water-level variability. In the present study, the late period salinity increase was greatest near the coast and diminished inland. This spatial pattern is consistent with stronger coastal influence, but the analysis does not directly determine whether the inland extent of salinity exposure changed.

The freshwater and other environmental variables tested here did not explain the observed spatial pattern as strongly as tidal amplitude and storm surge under the selected models. These results describe comparative associations and do not exclude freshwater availability, drought, storms, or correlated environmental processes as contributors.

Tidal amplitude and storm surge are derived from the same water-level records and may represent overlapping processes. The sustained association with amplitude is consistent with a persistent water-level influence, whereas storm surge represents episodic conditions. Additional process-based or temporally resolved analysis would be needed to distinguish these mechanisms and establish attribution.

6. Limitations and future work

6.1. Limitations

While our analysis describes where salinity change in the basin is concentrated, several limitations still remain. First, each station is expressed relative to a coastal reference drawn from the same network, so the reference shares the basin’s environmental settings rather than acting as a true representative of Gulf salinity. The reference station was selected for stability but carries a trend of its own. Because the coastal reference rose slightly over this interval, the ratio understates the true magnitude of the salinity increase. However, the absolute salinity gradient still reproduces an increasing trend, so the finding does not depend on the normalization.

Second, the study period begins when the continuous network reached usable coverage, so the reference frame is arbitrary. The gradient is significant for every start year from 2007 to 2021, and the 2010 start year provides one of the shallower estimates, so the reported gradient is conservative.

Third, we cannot determine whether a potential driver tracks distance or the true salinity intrusion. If distance acts through a driver, controlling the impact of these environmental drivers could remove real correlation, therefore removing a part of the true magnitude of drivers. The driver results are therefore a description, not an attribution.

Fourth, the late increase is characterized by a comparison of time blocks rather than by a change point. Monthly salinity is strongly autocorrelated, and this study does not estimate a formal change point or onset date. Instead, the late increase is described using a comparison of the 2010–2021 and 2022–2025 blocks. Trends within the later block alone are also not reported because the sign of the trend depends on the month chosen as its start.

Fifth, for the pre-2010 comparison, grab samples are collected infrequently and may contain many repeated values, which may pull the slope toward zero. Also, those records could be tested only in absolute salinity, so a spatial pattern is established only for continuous monitoring.

Finally, we did not model water-management interventions. Davis Pond diversion discharge accounts for a negligible share of the observed change, but the basin's freshwater configuration is treated as fixed. However, the Mid-Barataria Sediment Diversion was terminated in 2025 without operating (CPRA, 2025), and the results should not be extended past a change in that configuration.

Despite these limitations, our analysis establishes that the rate of salinity change in this basin is organized by distance from the shoreline. The spatial gradients complement process-based studies of the same system and are transferable to other tidally influenced basins.

6.2. Future work

Continued monitoring will extend the record, and repeating the analysis as the network accumulates further data will indicate whether the spatial gradient reported here steepens, remains relatively unchanged, or flattens over time. Denser station coverage, specifically in the middle of the basin, would resolve the shape of decay rather than only its slope. Direct measurements of potential drivers within the basin would allow the same comparison to test attribution rather than association. Furthermore, the water-level driver is computed from each station’s own sensor, so modeled water levels from a hydrodynamic reanalysis would separate regional hydrodynamic exposure from measurements made by each station’s own sensor, and a transport model of the same basin could test whether tidal exchange transports salt inland, rather than only raising the water level there. Finally, further research should focus on determining a suitable offshore monitoring station that would let the ratio be computed against Gulf salinity directly.

7. Conclusions

This study finds that the rate of salinity change in the Barataria Basin varies with distance from the shoreline, with the greatest increases occurring near the coast. Furthermore, this pattern was already present before the recent major increase, which demonstrates that the recent increase amplified an existing difference in salinity. The records therefore constrain where the basin is most exposed more tightly than they constrain what has driven the change. Anticipating further change in this basin will require process-based treatment of tidal exchange and wetland loss, along with a longer salinity record to establish whether the trend persists.

CRediT authorship contribution statement

Aaron Wang: Conceptualization, Methodology, Software, Formal analysis, Investigation, Data curation, Writing – original draft; Writing – review and editing, Visualization.

Declaration of competing interest

The author declares that they have no known competing financial interests or personal relationships that could have appeared to influence the work reported in this paper.

Acknowledgments

The author thanks the Louisiana Coastal Protection and Restoration Authority for maintaining the Coastwide Reference Monitoring System, the Louisiana Department of Wildlife and Fisheries for providing the fishery independent monitoring records, and the U.S. Geological Survey for providing the National Water Information System gauge data used in this analysis. This research received no external funding. All errors remain the author's own.

Data availability

All data used in this study are publicly available. CRMS hourly hydrographic data are available from CPRA's Coastal Information Management System at https://cims.coastal.louisiana.gov. Long-term salinity records from the Louisiana Department of Wildlife and Fisheries are available on request from LDWF. USGS gauge records are available from the National Water Information System at https://waterdata.usgs.gov/nwis. Turner transect data are archived at GRIIDC (Turner, 2017; https://doi.org/10.7266/N7736NZ9).

References

Baron, R.M., Kenny, D.A., 1986. The moderator–mediator variable distinction in social psychological research. J. Pers. Soc. Psychol. 51 (6), 1173–1182. https://doi.org/10.1037/0022-3514.51.6.1173

Benjamini, Y., Hochberg, Y., 1995. Controlling the false discovery rate: a practical and powerful approach to multiple testing. J. R. Stat. Soc. B 57 (1), 289–300. https://doi.org/10.1111/j.2517-6161.1995.tb02031.x

Blum, M.D., Roberts, H.H., 2009. Drowning of the Mississippi Delta due to insufficient sediment supply and global sea-level rise. Nat. Geosci. 2 (7), 488–491. https://doi.org/10.1038/ngeo553

Byrnes, M.R., Britsch, L.D., Berlinghoff, J.L., Johnson, R., Khalil, S., 2019. Recent subsidence rates for Barataria Basin, Louisiana. Geo-Mar. Lett. 39 (4), 265–278. https://doi.org/10.1007/s00367-019-00573-3

Cheng, F.Y., Van Meter, K.J., Byrnes, D.K., Basu, N.B., 2020. Maximizing US nitrate removal through wetland protection and restoration. Nature 588, 625–630. https://doi.org/10.1038/s41586-020-03042-5

Chesney, E.J., Baltz, D.M., Thomas, R.G., 2000. Louisiana estuarine and coastal fisheries and habitats: perspectives from a fish's eye view. Ecol. Appl. 10 (2), 350–366. https://doi.org/10.2307/2641098

Coastal Protection and Restoration Authority (CPRA), 2022. Coastal Information Management System (CIMS) Data Dictionary. https://cims.coastal.louisiana.gov/RecordDetail.aspx?Root=0&sid=11505

Coastal Protection and Restoration Authority (CPRA), 2025. State, Louisiana Trustee Implementation Group announce termination of Mid-Barataria Sediment Diversion funding. Press release, 17 July 2025. https://coastal.la.gov/news/state-louisiana-trustee-implementation-group-announce-termination-of-mid-barataria-sediment-diversion/

Couvillion, B.R., Beck, H., Schoolmaster, D., Fischer, M., 2017. Land area change in coastal Louisiana (1932 to 2016). U.S. Geological Survey Scientific Investigations Map 3381. http://pubs.er.usgs.gov/publication/sim3381

Das, A., Justic, D., Inoue, M., Hoda, A., Huang, H., Park, D., 2012. Impacts of Mississippi River diversions on salinity gradients in a deltaic Louisiana estuary: ecological and management implications. Estuar. Coast. Shelf Sci. 111, 17–26. https://doi.org/10.1016/j.ecss.2012.06.005

Day, J.W., Martin, J.F., Cardoch, L., Templet, P.H., 1997. System functioning as a basis for sustainable management of deltaic ecosystems. Coast. Manag. 25 (2), 115–153. https://doi.org/10.1080/08920759709362315

Day, J.W., Britsch, L.D., Hawes, S.R., Shaffer, G.P., Reed, D.J., Cahoon, D., 2000. Pattern and process of land loss in the Mississippi Delta: a spatial and temporal analysis of wetland habitat change. Estuaries 23 (4), 425–438. https://doi.org/10.2307/1353136

Edmonds, D.A., Toby, S.C., Siverd, C.G., Twilley, R., Bentley, S.J., Hagen, S., Xu, K., 2023. Land loss due to human-altered sediment budget in the Mississippi River Delta. Nat. Sustain. 6 (6), 644–651. https://doi.org/10.1038/s41893-023-01081-0

Hirsch, R.M., Slack, J.R., Smith, R.A., 1982. Techniques of trend analysis for monthly water quality data. Water Resour. Res. 18 (1), 107–121. https://doi.org/10.1029/WR018i001p00107

Hu, K., Meselhe, E.A., Reed, D.J., 2023. Understanding drivers of salinity and temperature dynamics in Barataria Estuary, Louisiana. J. Geophys. Res. Oceans 128 (7), e2023JC019635. https://doi.org/10.1029/2023JC019635

Inoue, M., Park, D., Justic, D., Wiseman, W.J., 2008. A high-resolution integrated hydrology–hydrodynamic model of the Barataria Basin system. Environ. Model. Softw. 23 (9), 1122–1132. https://doi.org/10.1016/j.envsoft.2008.02.011

Kang, B., Xie, S., 2024. Enhanced tidal intrusion in the Barataria Basin, Mississippi River Delta. J. Coast. Res. 41 (2), 336–346. https://doi.org/10.2112/JCOASTRES-D-24-00047.1

Kang, B., Xie, S., 2025. Accelerated land loss and nuisance flooding potential in the Barataria Basin: the impacts of land subsidence, sea-level rise, and tidal dynamics. J. Sea Res. 205, 102594. https://doi.org/10.1016/j.seares.2025.102594

Khalifa, A.M., Meselhe, E.A., Hu, K., Reed, D., Azim Beg, M.N., 2024. Development and application of a simplified biophysical model to study deltaic and coastal ecosystems. Estuar. Coast. Shelf Sci. 306, 108899. https://doi.org/10.1016/j.ecss.2024.108899

Landsea, C.W., Franklin, J.L., 2013. Atlantic hurricane database uncertainty and presentation of a new database format. Mon. Weather Rev. 141 (10), 3576–3592. https://doi.org/10.1175/MWR-D-12-00254.1

Lee, J., Biemond, B., van Keulen, D., Huismans, Y., van Westen, R.M., de Swart, H.E., Dijkstra, H.A., Kranenburg, W.M., 2025. Global increases of salt intrusion in estuaries under future environmental conditions. Nat. Commun. 16, 3444. https://doi.org/10.1038/s41467-025-58783-6

Louisiana Department of Wildlife and Fisheries (LDWF), 2019. Marine Fisheries Section Independent Sampling Activities Field Manual, December 2018 update. LDWF, Baton Rouge, LA. https://pub-data.diver.orr.noaa.gov/restoration/LDWF%20Marine%20Fisheries%20Independent%20Sampling%20Activities%20Field%20Manual%202018-12%20UPDATE%20(2019-11-29).pdf

Mann, H.B., 1945. Nonparametric tests against trend. Econometrica 13 (3), 245–259. https://doi.org/10.2307/1907187

Marchetto, A., 2024. rkt: Mann-Kendall test, Seasonal and Regional Kendall tests. R package version 1.7. https://doi.org/10.32614/CRAN.package.rkt

Massicotte, P., South, A., 2026. rnaturalearth: World map data from Natural Earth. R package version 1.2.0. https://doi.org/10.32614/CRAN.package.rnaturalearth

Nienhuis, J.H., Törnqvist, T.E., Jankowski, K.L., Fernandes, A.M., Keogh, M.E., 2017. A new subsidence map for coastal Louisiana. GSA Today 27 (9), 58–59. https://doi.org/10.1130/GSATG337GW.1

Pebesma, E., 2018. Simple Features for R: standardized support for spatial vector data. R J. 10 (1), 439–446. https://doi.org/10.32614/RJ-2018-009

R Core Team, 2026. R: A language and environment for statistical computing, version 4.6.0. R Foundation for Statistical Computing, Vienna, Austria. https://www.R-project.org/

Rahman, M.M., Penny, G., Mondal, M.S., Zaman, M.H., Kryston, A., Salehin, M., Nahar, Q., Islam, M.S., Bolster, D., Tank, J.L., Müller, M.F., 2019. Salinization in large river deltas: drivers, impacts and socio-hydrological feedbacks. Water Secur. 6, 100024. https://doi.org/10.1016/j.wasec.2019.100024

Sen, P.K., 1968. Estimates of the regression coefficient based on Kendall's tau. J. Am. Stat. Assoc. 63 (324), 1379–1389. https://doi.org/10.1080/01621459.1968.10480934

Steyer, G.D., Sasser, C.E., Visser, J.M., Swenson, E.M., Nyman, J.A., Raynie, R.C., 2003. A proposed coast-wide reference monitoring system for evaluating wetland restoration trajectories in Louisiana. Environ. Monit. Assess. 81, 107–117. https://doi.org/10.1023/A:1021368722681

Turner, R.E., 2017. Water quality data from the Barataria Basin, 1994–2016. Gulf of Mexico Research Initiative Information and Data Cooperative (GRIIDC), Harte Research Institute, Texas A&M University–Corpus Christi. https://doi.org/10.7266/N7736NZ9

Visser, J.M., Sasser, C.E., Chabreck, R.H., Linscombe, R.G., 1998. Marsh vegetation types of the Mississippi River deltaic plain. Estuaries 21 (4), 818–828. https://doi.org/10.2307/1353283

Vose, R.S., Applequist, S., Squires, M., Durre, I., Menne, M.J., Williams, C.N., Fenimore, C., Gleason, K., Arndt, D., 2014. Improved historical temperature and precipitation time series for U.S. climate divisions. J. Appl. Meteorol. Climatol. 53 (5), 1232–1251. https://doi.org/10.1175/JAMC-D-13-0248.1

Wiseman, W.J., Swenson, E.M., Power, J., 1990. Salinity trends in Louisiana estuaries. Estuaries 13 (3), 265–271. https://doi.org/10.2307/1351917